


Charge trapping at Al/Al₂O₃ interface facilitates hydrogen-induced superabundant metal vacancy formation

Vrinda Somjit¹ and Bilge Yildiz^{1,2,*}

¹Department of Materials Science and Engineering, Massachusetts Institute of Technology, Cambridge, Massachusetts 02139, USA

²Department of Nuclear Science and Engineering, Massachusetts Institute of Technology, Cambridge, Massachusetts 02139, USA

 (Received 7 February 2023; revised 23 May 2023; accepted 23 June 2023; published 25 July 2023)

Hydrogen is a ubiquitous impurity that deteriorates the metal/oxide interface, causing challenges such as current leakage and blistering. Here, we uncover the mechanisms behind hydrogen-induced damage at the prototypical Al/Al₂O₃ interface. The precursor that we identify is charge trapping at the interface, which facilitates hydrogen segregation to the interface plane as H⁻. Presence of hydrogen increases aluminum vacancy concentration at the interfacial metal and oxide planes. Each Al vacancy can trap multiple hydrogen atoms. As a result, the interfacial aluminum vacancy and hydrogen concentrations increase by orders of magnitude. Additionally, hydrogen behaves as an *n*-type dopant and increases electronic conductivity at the oxide layer adjacent to the interface by forming H⁺, and the [V_{Al}-H] complex is the predominant defect at this layer. These findings provide the precursor mechanisms of hydrogen-induced damage at the metal-oxide interfaces and have implications for advancing Al/Al₂O₃-based coatings and electronic devices.

DOI: [10.1103/PhysRevMaterials.7.L072001](https://doi.org/10.1103/PhysRevMaterials.7.L072001)

The Al/Al₂O₃ interface is a canonical metal-oxide interface and is utilized in important applications, including protective coatings [1–4], micro-/nanoelectronics [5–7], composites [1,8], catalyst supports [9], and hydrogen production [10]. The integrity of the interface and the electronic conductivity of the oxide play a critical role in the performance of these applications. Hydrogen, a ubiquitous impurity commonly found in most processing and operating environments, can incorporate into Al₂O₃ and Al, affecting these key properties. For example, hydrogen accumulation at the Al/Al₂O₃ interface is thought to cause blistering and spallation of the protective oxide, deteriorating protectiveness of the coating [11–14]. Hydrogen incorporation is known to increase the leakage current in Al/Al₂O₃/Al tunnel junctions, leading to poor performance and device failure [15–17]. Hydrogen is also a two-level system in Al/Al₂O₃-based superconducting qubits, especially near surfaces and interfaces, leading to quantum decoherence [18–20].

Despite this pervasive effect of hydrogen on Al/Al₂O₃-based devices and coatings, atomic-level understanding of the underlying mechanisms is still lacking. For example, it is unclear whether hydrogen-induced structural damage is initiated at the oxide side or the metal side of the interface. First-principles studies propose interfacial blistering is mainly initiated by breaking of interfacial Al_{metal}-O bonds by hydrogen, and hydrogen accumulation in subinterfacial cation vacancies in the oxide [12]. In contrast, experimental studies indicate that damage likely begins at the metal side, facilitated by interfacial weakening due to hydrogen and the resulting metal diffusion-induced interfacial cavitation [11]. The reason behind the increase in electronic conductivity upon hydrogen incorporation in Al₂O₃ films on Al is also

unclear. First-principles calculations suggest that nonbonded H interstitials [15] mediate electron tunneling through the oxide, whereas anodic polarization experiments indicate that the increase in conductivity is likely due to electron donation by the formation of positively charged defects [15,17] (such as H⁺). Finally, in the context of two-level systems in Al/Al₂O₃ superconducting qubits, first-principles calculations have only simulated hydrogen in bulk Al₂O₃, with different studies [19,20] attributing decoherence to different hydrogen defect species, such as H⁺ interstitials [20] and [V_{Al}-H]^q complexes (where *q* = charge state of complex) [19]. This highlights that explicit atomistic simulation of H defects at the interface between Al and Al₂O₃ would be desirable to reconcile these inconsistencies.

Here, we find that electronic charge trapped at the Al/Al₂O₃ interface causes hydrogen segregation to the interface. The segregation of hydrogen then reduces the formation energies of aluminum vacancies at the interfacial metal plane. This leads to the formation of superabundant vacancies, which in turn trap multiple hydrogen atoms. This self-catalytic mechanism is the likely precursor mechanism to cavitation and blistering at the interface. We also find that hydrogen forms H⁺ at the oxide layer adjacent to the interface by donating its electron to the interfacial midgap states, which could explain the increase in conductivity of thin Al₂O₃ films. Last, we find that the [V_{Al}-H] complex is the predominant defect in this layer, which could be an important consideration for decoherence in superconducting qubits.

Details about the interface structure simulated [21], simulation technique [including parameters of our density-functional theory (DFT) calculations] and defect-formation energy calculations, are given in Supplemental Material, Secs. 1 and 2 [22] (see also Refs. [23–43] therein). Specifically, the interface structure identified by *ab initio* grand canonical Monte Carlo (GCMC) under Al-rich, O-poor conditions (the

*Corresponding author: byildiz@mit.edu

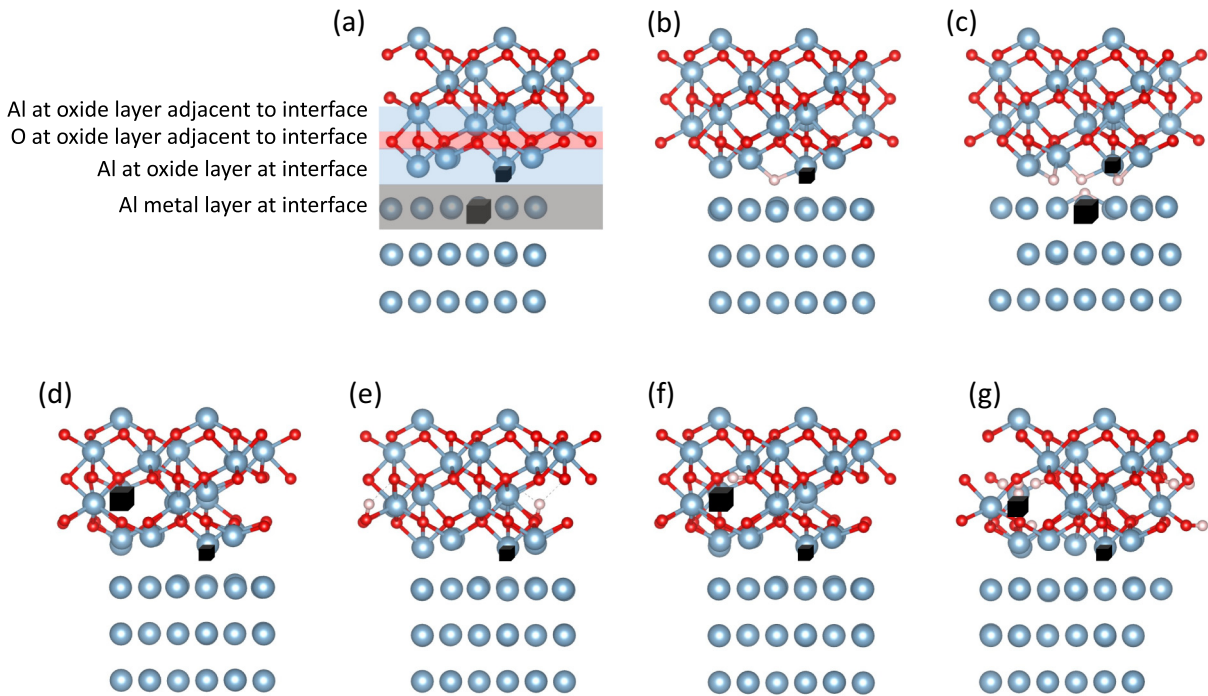


FIG. 1. Relaxed structures of key defects at interface (a)–(c) and at oxide layer adjacent to interface (d)–(g). Note that oxide layer at interface has 12.5% V_{Al} as found from *ab initio* GCMC calculations [21]. We depict this “intrinsic” vacancy as a small black cube to differentiate it from “extrinsic” vacancies that we investigate in this study. We represent the latter as a large black cube. (a) V_{Al} , (b) H_{O} , (c) $[\text{V}_{\text{Al}}\text{-4H}]$ at interfacial metal layer (d) V_{Al} , (e) H_{int} , (f) $[\text{V}_{\text{Al}}\text{-H}]$, and (g) $[\text{V}_{\text{Al}}\text{-5H}]$ at oxide layer adjacent to interface. Only layers near interface are shown. Red spheres: oxygen; blue spheres: aluminum; and white spheres: hydrogen. (a) also denotes nomenclature for different regions at which defects were investigated.

conditions we expect at the equilibrated Al/Al₂O₃ interface from our previous work [21]) was used in this study. Al₂O₃ (0001) is strained in plane to match the lattice parameters of Al (111), resulting in a misfit strain of $\sim 3\%$ (see Supplemental Material, Sec. 1 for additional details [22]). The computed Al 2*p* and O 1*s* interfacial core-level shifts of this interface closely match that of experiments, as discussed in Ref. [21], thereby making this a realistic interface structure to base our investigations upon. Defects investigated in this work include hydrogen bonded to interfacial undercoordinated Al (Al “dangling bonds”) from the oxide, hydrogen on fcc hollow sites at the interfacial metal layer, aluminum vacancies and aluminum vacancy–hydrogen complexes at the metal layer and oxide layer adjacent to the interface, and aluminum divacancies and their complexes with hydrogen at the interfacial metal layer. The relaxed structures of key defects studied are shown in Fig. 1.

Our first key observation is that hydrogen segregates to the interface with a segregation energy of 0.39 eV from the metal side and 3.2 eV from the oxide side ($E_{\text{seg}} = E_{f, \text{H in metal or oxide}} - E_{f, \text{H at interface}}$, where E_{seg} and E_f are the segregation and formation energies respectively, with $E_{f, \text{H in metal or oxide}}$ computed from separate simulations of H defects in bulk Al and bulk Al₂O₃; see Supplemental Material, Sec. S2 for more details [22]). Note that the segregation energy from the oxide side is an order of magnitude higher than from the metal due to the high formation energy of H interstitial in the oxide compared to the metal. We tested several sites for hydrogen stability as detailed in Supplemental

Material, Sec. S3 [22]. Interestingly, H does not form H⁺ and break interfacial Al–O bonds to bond with O at the interface. Instead, hydrogen is stable only either at the fcc hollow sites on the Al metal layer at the interface (H_{fcc}) or bonds with the undercoordinated Al atoms at the oxide side of the interface, i.e., at the oxygen site (H_{O}). In both cases, H has a calculated Bader charge [44,45] of ~ -2 , i.e., it exists as H[−].

This segregation of H to the interface can be understood by examining the electronic structure of the interface and the charge redistribution that occurs upon the addition of hydrogen at the interface. In our previous study on the Al/Al₂O₃ interface [21], Bader charge [44,45] analysis [Fig. 2(a)] revealed that the interfacial Al atoms on the oxide side [labeled as layer Al4 in Fig. 2(c)] on average each have one extra electron (compared to Al³⁺) due to undercoordination. These excess electrons are accommodated in the midgap states made of Al 3*s*, 3*p* and O 2*p* from the oxide layer near the interface. This contribution of the interfacial Al atoms from the oxide side [Al4 layer in Fig. 2(c)] to the midgap states can be seen in Fig. 2(b) (top projected density of states (PDOS) panel labeled “Al4, no H”; see also Fig. 4 in Ref. [21]). In fact, this is reminiscent of an electride, where the electrons are spatially separated from the positively charged ions [46]. Upon introducing H at the interface, the H 1*s* orbital interacts strongly with these interfacial Al 3*s**p* dangling bonds to form H[−] and therefore is trapped in stable Al–H bonds at the interface. This bond formation can be seen in the projected density of states plot in Fig. 2(b), where peaks made from the superposition of H and Al states (from interfacial Al4 layer) are seen deep

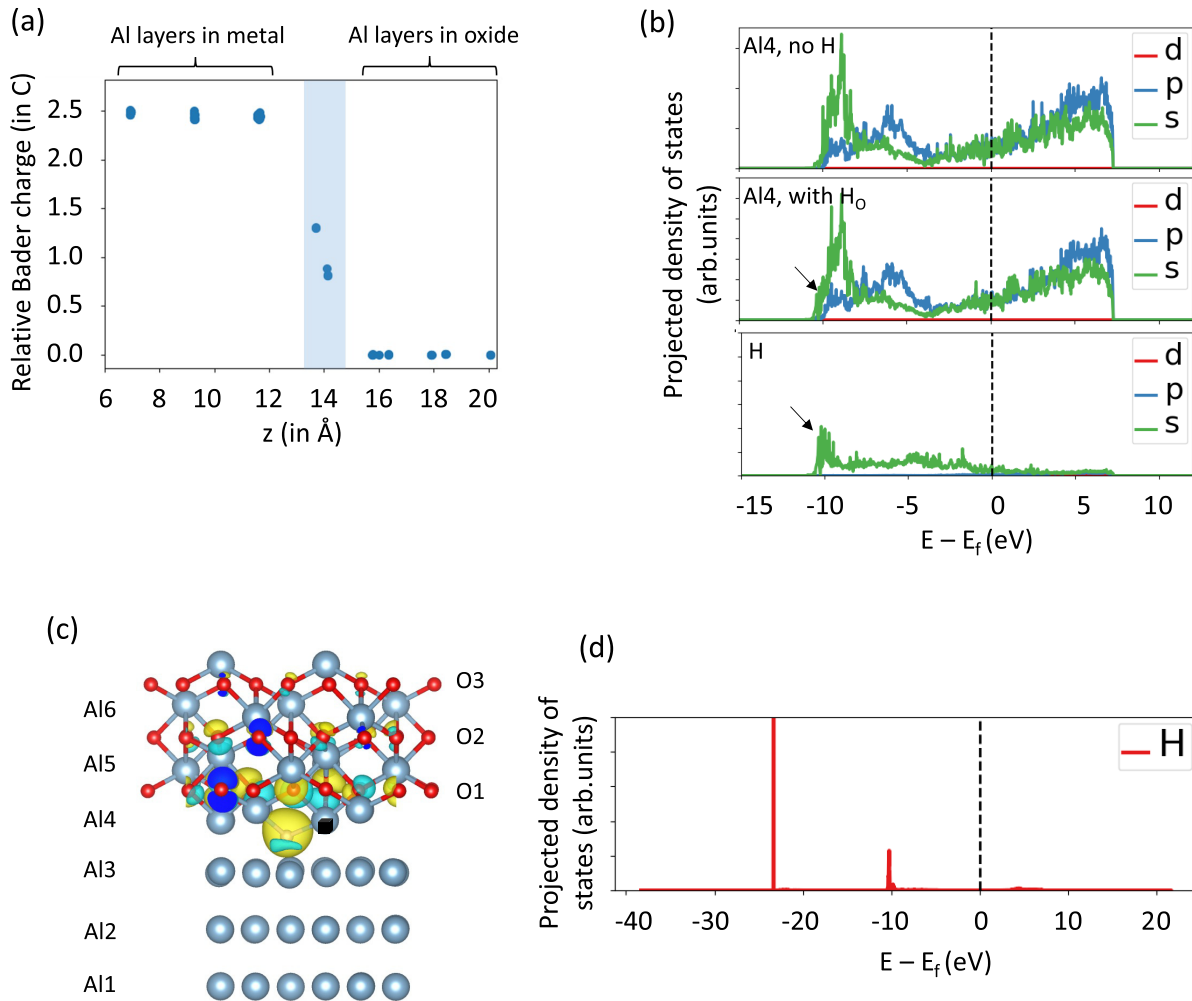


FIG. 2. (a) Relative Bader charge (q_{rel}) on Al as a function of its position in Al/Al₂O₃ simulation cell ($q_{\text{rel}} = q_{\text{Al}} - q_{\text{Al in Al}_2\text{O}_3 \text{ bulk}}$, where q_{Al} is Bader charge on Al and $q_{\text{Al in Al}_2\text{O}_3 \text{ bulk}}$ is Bader charge on Al in bulk Al₂O₃). (b) From top to bottom: Projected density of states (PDOS) of interfacial Al at oxide side (Al4 layer) without H defect; PDOS of interfacial Al at oxide side (Al4 layer) with H₀ defect; PDOS of H defect. Overlapping Al and H PDOS are marked with an arrow. Spin-up PDOS is shown, with Fermi level at 0 eV. (c) Charge-density difference (between interface with H₀ and bare interface) plot, revealing bonding between undercoordinated Al cations and H. Only layers near interface are shown. Oxide layer at interface has 12.5% V_{Al} as found from *ab initio* GCMC calculations [21], depicted as a small black cube. (d) PDOS of H⁺ defect formed upon H donating its electron to midgap states and forming an O–H bond, shown by PDOS peak in valence band. Spin-up PDOS is shown. Resulting structure is shown in Fig. 1(e).

in the valence band (at -9 to -11 eV). Figure 2(c) plots the charge-density difference between the interface with H₀ and the bare interface (i.e., $\rho_{\text{interface with H}_0} - \rho_{\text{bare interface}}$), showing the bond formation between undercoordinated interfacial cations and H. Crucially, this also explains why interfacial O–H bonds are not formed: H prefers to segregate to sites with high electron density to form H[−] and a bonding state in the valence band, thus forming strong Al–H bonds, rather than form H⁺ and weaken an existing Al–O bond to form a covalent O–H bond. Monte Carlo simulations with different H concentrations at different equilibrium interface structures found in our previous study [21] confirm this behavior (Supplemental Material, Sec. S4 [22]). While we have not explicitly quantified the effect of Al₂O₃ thickness on H-defect formation at the interface, the Monte Carlo simulations show that H-segregation behavior is likely a very local effect, confined to the interfacial plane, and therefore is likely independent of

the thickness or phase of the oxide layer. Note that similar H multicenter bond formation upon H substitution on an oxygen site has been reported in metal oxides like MgO and ZnO [47].

While the excess charge accommodated in the interfacial midgap states help stabilize H as H[−] at the interface, the remaining unoccupied midgap states help stabilize H as H⁺ in the oxide layer adjacent to the interface, as shown in Fig. 1(e). In contrast to bulk Al₂O₃, where neutral H is a $-U$ center [48,49] and H⁺ or H[−] will form only in the presence of other acceptor or donor defects (respectively), the presence of empty midgap states in the oxide layer adjacent to the interface aid in the formation and stabilization of H⁺ in that layer. From the density of states (DOS) plot in Fig. 2(d), we see that H prefers to form H⁺ and an O–H bond, as seen in the DOS peak deep in the valence band. Thus, the energetic stability from the formation of an O–H bond and the presence of empty midgap states near the H-defect level results in the

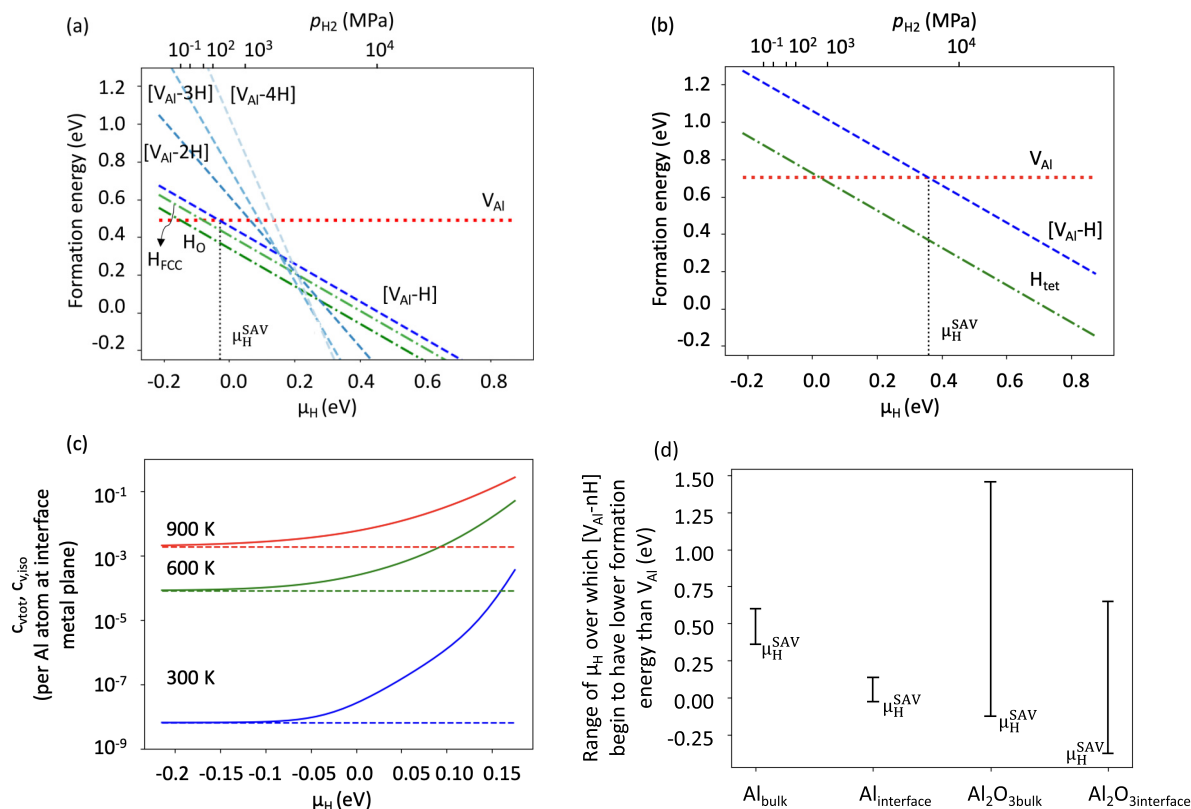


FIG. 3. Formation energy of hydrogen and aluminum vacancy (V_{Al}) defects as function of hydrogen chemical potential, μ_H : (a) at metal layer of interface and (b) in bulk Al. μ_H is shown using $\frac{1}{2}(\mu_{H_2}^0)$ as reference, where $\mu_{H_2}^0$ is the chemical potential of a H_2 molecule at 0 K, i.e., the DFT energy of a H_2 molecule. Corresponding partial pressure of hydrogen gas at 300 K is shown in MPa. Vertical dotted line in (a) and (b) marks μ_H at which onset of SAV formation occurs (-0.03 and 0.36 eV, at interface vs in metal, respectively). (c) Aluminum vacancy concentration at interfacial metal layer as function of hydrogen chemical potential at 300, 600, and 900 K. Dotted lines denote total concentration of isolated aluminum vacancy on interfacial metal plane ($c_{v,iso}$) and solid lines denote total aluminum vacancy concentration ($V_{Al} + [V_{Al}-nH]$) on interfacial metal plane ($c_{v,tot}$). Note how the aluminum vacancy concentration begins to increase rapidly at ~ -0.03 eV. Note that as long as $\mu_H > \mu_H^{SAV}$, $[V_{Al}-nH]$ complex concentration will be higher than isolated V_{Al} irrespective of temperature, as formation energies of complexes are lower than isolated V_{Al} , as seen in (a). (d) Summarizing range of μ_H in bulk Al, at interfacial metal layer, in bulk Al_2O_3 , and at oxide layer adjacent to interface, over which $[V_{Al}-nH]$ complexes begin to have lower formation energies than isolated V_{Al} . Lower bound of each range is μ_H at which onset of SAV formation occurs.

formation of H^+ in the oxide layer adjacent to the interface, without requiring the presence of any acceptor defects.

Our second key observation is that the segregation of H to the interface results in the increase in the concentration of aluminum vacancies at the interfacial metal layer through the formation of $[V_{Al}-H]$ complexes. This is explained through Figs. 3(a) and 3(b), which plot the formation energies of V_{Al} , H, and $[V_{Al}-H]$ defects at the interfacial metal layer and in bulk aluminum, respectively, as a function of hydrogen chemical potential μ_H . Note that by plotting the formation energies over a range of μ_H , our results are agnostic to the particular hydrogen-charging mechanism (for example, exposure to hydrogen gas, hydrogen plasma, electrolytic charging with hydrogen, immersion in water, etc.) [50]. Thus, one can calculate the μ_H under different experimental conditions and map it back onto this plot to identify the formation energies and concentrations of different defects.

As μ_H is increased, the formation energy of isolated H defects and $[V_{Al}-H]$ complexes decreases, as expected. However, we also notice that beyond $\mu_H = -0.03$ eV at the

interface [Fig. 3(a)] and 0.36 eV in bulk metal Al [Fig. 3(b)], the formation energy of $[V_{Al}-H]$ is lower than isolated V_{Al} . This indicates that at hydrogen chemical potentials greater than -0.03 eV (for Al/ Al_2O_3 system) and 0.36 eV (for bulk Al), hydrogen lowers the formation energy of V_{Al} through the formation of $[V_{Al}-H]$ complexes. This increases the absolute concentration of aluminum vacancies, much higher than the concentrations obtained in the absence of hydrogen, as shown in Fig. 3(c) for V_{Al} concentrations at the interfacial metal layer at different temperatures (see Supplemental Material, Sec. S5 [22] for a discussion on how the concentrations were calculated).

This is consistent with the phenomenon called the superabundant vacancy (SAV) formation in bulk metals, which was first experimentally observed in Pd and Ni [51] and later in other metals such as Cu [52], Al [53], and Fe [54]. Superabundant vacancy formation occurs when the trapping of hydrogen in the metal vacancy leads to an overall reduction in the energy of formation of the vacancy [55]. This causes the vacancy concentration to increase by several orders of magnitude [55].

TABLE I. Binding energies of [V_{Al}-nH] complexes, with V_{Al} at interfacial metal layer (column 1) and V_{Al} at oxide layer adjacent to interface (column 2). Column 3 shows binding energies of Al divacancies and their complexes with hydrogen.

Complex	E_b (eV)	Complex	E_b (eV)	Complex	E_b (eV)
[V _{Al} -H]	0.37	[V _{Al} -H]	2.28	[V _{Al} -V _{Al}]	-0.08
[V _{Al} -2H]	0.18	[V _{Al} -2H]	1.22	[[V _{Al} -H]-[V _{Al} -H]]	-0.04
[V _{Al} -3H]	0.18	[V _{Al} -3H]	0.44	[[V _{Al} -2H]-[V _{Al} -2H]]	0.40
[V _{Al} -4H]	0.07	[V _{Al} -4H]	1.63		
		[V _{Al} -5H]	0.70		
		[V _{Al} -6H]	0.02		

DFT analysis has shown that the broken bonds due to undercoordinated metal atoms around the vacancy are highly reactive and therefore are favorably terminated by H. This gives rise to stabilization of metal vacancies, as well as trapping of H at the vacancy site [55,56].

An important difference here is that the onset μ_H for SAV formation at both the metal and oxide sides of the interface is much lower than in bulk Al and in bulk Al₂O₃. As shown in Fig. 3(b) and discussed above, SAVs in bulk Al begin to form at $\mu_H^{\text{SAV}} \sim 0.36$ eV, i.e., 0.39 eV higher than interfacial μ_H^{SAV} . In fact, $\mu_H^{\text{SAV}} \sim 0.36$ eV indicates that formation of SAVs in bulk Al is unlikely [55], as bulk fcc Al transforms to AlH₃ at ~ 700 MPa ($\mu_H \sim 0.01$ eV in Fig. 3) [57–59] at 300 K. In contrast, $\mu_H^{\text{SAV}} \sim -0.03$ eV at the interface indicates that SAVs readily form at the interfacial metal layer, before the transformation of Al to AlH₃. Comparing the shift in μ_H^{SAV} (0.39 eV) with the H-segregation energy (0.39 eV) to the interface, we see that the segregation energy is responsible for the shift in μ_H^{SAV} , thereby lowering the onset μ_H for SAV formation and drastically increasing the [V_{Al}-H] concentration at the interface.

SAV formation can also lead to a rapid increase in H concentration by the trapping of multiple H atoms in the vacancies to form [V_{Al}-nH] complexes (where n is the number of H atoms trapped in V_{Al}) [50,55,60]. Such [V_{Al}-nH] complexes in bulk Al have been investigated in prior studies [50,55] and may have important consequences for hydrogen embrittlement of Al [50,55,60]. We similarly tested the H-trapping effect of V_{Al} at the interfacial metal layer and the formation of [V_{Al}-nH] complexes. The binding energy of hydrogen to V_{Al} (or to an existing [V_{Al}-($n-1$)H] complex) at the interfacial metal layer was calculated as

$$E_b([V_{\text{Al}} - n\text{H}]) = E_f([V_{\text{Al}} - (n-1)\text{H}]) + E_f(\text{H}_\text{O}) - E_f([V_{\text{Al}} - n\text{H}]), \quad (1)$$

i.e., this is the formation energy of an isolated interfacial V_{Al} (or [V_{Al}-($n-1$)H] complex) and H_O relative to that of the complex [V_{Al}-nH]. We evaluated the binding energy of a single H atom at different sites and different distances from V_{Al} (shown in Supplemental Material, Sec. S6 [22]), and checked for the possibility of formation of [V_{Al}-nH] complexes by the sequential filling of the sites with favorable (positive) E_b , testing various configurations.

Table I (column 1) shows that it is energetically favorable to trap 4 H atoms in V_{Al} at the interface metal layer, each H occupying either an H_O or the H_{fcc} site. Thus, under high H loading, nonequilibrium conditions where binding energies

play an important role in determining the concentration of defects and their complexes [48,50,61], the positive binding energies in Table I indicate that [V_{Al}-nH] complexes can form. Thus, not only can SAV formation readily occur at the interface, which increases the V_{Al} concentration at the interface metal layer by orders of magnitude; additionally, each resulting V_{Al} from SAV formation can trap multiple H, increasing the effective H concentration at the interface. Together, the rapid increase in V_{Al} and H concentrations can act as precursors to cavitation and blistering of the interface. This enhanced local H concentration may also promote hydride formation at the interface.

We find that hydrogen has similar effects at the oxide layer adjacent to the interface, where it lowers the formation energy for aluminum vacancies by the formation of [V_{Al}-nH] complexes, and can also accumulate at the aluminum vacancies, as shown in Supplemental Material, Sec. S7 [22]. Cation vacancies, such as those in ZrO₂ [62] and Al₂O₃ [12,48], are known to have a strong tendency to accumulate hydrogen. This is because hydrogen prefers to donate its electron to the acceptor states introduced by the cation vacancy (i.e., holes on the oxygen ions surrounding the vacancy), forming O–H bonds [62]. This gives rise to a large binding energy of the cation vacancy–hydrogen defect complex. From Supplemental Material, Fig. S5 [22], the defect complex of V_{Al} with 1 H trapped is the most stable across a wide range of hydrogen chemical potentials and begins to have a lower formation energy than the isolated V_{Al} from $\mu_H = -0.26$ eV. Figure 1(f) shows the structure of this complex, where hydrogen forms O–H bonds with the oxygen atoms at nearest-neighbor sites to the V_{Al}. Table I (column 2) tabulates the binding energies of the [V_{Al}-nH] complexes at the oxide layer adjacent to the interface, indicating that a maximum of 5 H can be trapped at the V_{Al} (we do not consider V_{Al}-6H, which has E_b close to room temperature). The binding energy was calculated using Eq. (1), replacing $E_f(\text{H}_\text{O})$ with $E_f(\text{H}_{\text{int}})$ (the formation energy of an isolated H at the octahedral interstitial site at the oxide layer adjacent to the interface).

Figure 3(d) summarizes the discussion above. It plots the range of μ_H over which [V_{Al}-nH] complexes begin to have lower formation energies than isolated V_{Al} in the different systems, comparing the values in bulk to those at the interface. The lower bound of this range is the μ_H at which SAV onset occurs. The upper bound of this range is the maximum μ_H at which a [V_{Al}-nH] defect begins to have lower formation energy than isolated V_{Al}. The formation energy vs μ_H plot for [V_{Al}-nH] complexes in bulk Al₂O₃ [from which the μ_H range shown in Fig. 3(d) was extracted] is given in Supplemental

Material, Sec. S8 [22]. At the interface and at the oxide layer adjacent to the interface, the onset μ_H for SAVs are lower than their counterparts in bulk Al and Al_2O_3 ; additionally, $[\text{V}_{\text{Al}}-n\text{H}]$ complexes become more stable than V_{Al} at lower μ_H compared to their counterparts in bulk Al and Al_2O_3 . Note that the range for Al_{bulk} was taken from Nazarov *et al.* [55].

Finally, we also investigated aluminum divacancies at the interfacial metal layer. Divacancies are known to be unstable in bulk Al [60,63] but can be stabilized by the trapping of multiple H in each vacancy [60]. From the binding energies reported in Table I (column 3), similar to that in the Al bulk, Al divacancies are unstable at the interface. However, we find that trapping of 2 H in each vacancy can stabilize a divacancy at the interface. Thus, divacancies can favorably form at the hydrogenated interface, accelerating damage and acting as precursors to the formation of cavities and microvoids [11,14,60].

We now discuss the implications of this understanding of hydrogen behavior at the Al/ Al_2O_3 interface. We begin by noting that although the activation energy (E_a) for hydrogen diffusion in Al_2O_3 is very high ($E_a \sim 2.25$ eV in single-crystal Al_2O_3 [64]), hydrogen can still reach the interface via fast diffusion pathways such as dislocations, grain boundaries, or cracks in the Al_2O_3 layer (E_a in polycrystalline Al_2O_3 is ~ 1.89 eV [64]). Hydrogen can also reach the interface from the Al layer ($E_a \sim 0.46$ eV in single-crystal Al [65]). Ultimately, given that experiments (as discussed below and in the Introduction) report interfacial damage due to hydrogen present at the interface, our study provides insight into the potential causes behind this damage once the hydrogen reaches the interface.

In the context of coatings and passive oxide layers, the low formation energies of H_O and H_{fcc} at the interface indicate that when (if) hydrogen diffuses through the Al_2O_3 passivation layer and reaches the interface, it will remain trapped at the interface, and slow down hydrogen diffusion across this interface. This indicates that multilayer coatings with alternating layers of Al_2O_3 and Al could provide high hydrogen permeation resistance by trapping hydrogen at the interfaces. Some studies have alluded to this [66]. We also gain insight into the atomistic mechanisms that could initiate cavitation and blistering at the interface. Comparing the energetics of the different defects in the metal versus oxide sides of the interface, we see that the V_{Al} and $[\text{V}_{\text{Al}}-n\text{H}]$ defect formation

energetics at the Al metal side are much more favorable. Thus, damage most likely initiates at the Al side, due to H accumulation at the interface, SAV formation, and $[\text{V}_{\text{Al}}-n\text{H}]$ complex formation at the interfacial Al metal layer. The increased V_{Al} concentration due to SAV formation can weaken the interface and facilitate metal diffusion required for cavity formation and growth observed in experiments [11,14]. The increased hydrogen concentration can ultimately form hydrogen molecules, leading to bubbles and blistering, or even the formation of a hydride phase.

In the context of electronic devices, the increase in electronic conductivity observed upon hydration of Al/ Al_2O_3 /Al tunnel junctions could be due to the empty midgap states at the oxide layer adjacent to the interface accepting electrons from H to stabilize H^+ . Thus, the mechanism of H as an n -type dopant must be considered in conjunction with the increase in electronic conductivity due to tunneling via H defects as mentioned in prior work [15]. Our study also helps identify which hydrogen defects could be the predominant sources for decoherence in superconducting qubits. From our hydrogen defect-formation energies explicitly at different regions near the interface, we find that in the oxide layer adjacent to the interface, $[\text{V}_{\text{Al}}-\text{H}]$ has the least formation energy across the entire range of hydrogen chemical potential, and therefore has the highest concentration. Thus, it could be an important source of decoherence, as reported for bulk Al_2O_3 [19], along with H^+ in the octahedral interstitial site [20].

We thank Dr. Konstantin Klyukin and Dr. Pjotr Žgajnski for helpful discussions. This work has been supported by the U.S. Department of Energy, Office of Science, Office of Energy Efficiency and Renewable Energy, under Award No. DE-EE0008830. This work used the Extreme Science and Engineering Discovery Environment (XSEDE) resources [67] Stampede2 at the Texas Advanced Computing Center (TACC) and Expanse at the San Diego Supercomputer Center (SDSC) through Allocation No. TG-DMR120025. XSEDE is supported by National Science Foundation Grant No. ACI-1548562. This work also used FRONTIERA [68] at the Texas Advanced Computing Center through Allocation No. DMR20012. We thank the staff at TACC and SDSC for technical support.

V.S. performed the simulations; B.Y. supervised the work; both authors discussed the results and wrote the manuscript.

-
- [1] Z. Yin, S. Tao, X. Zhou, and C. Ding, Microstructure and mechanical properties of Al_2O_3 -Al composite coatings deposited by plasma spraying, *Appl. Surf. Sci.* **254**, 1636 (2008).
- [2] Y. Xin, C. Liu, W. Zhang, J. Jiang, G. Tang, X. Tian, and P. K. Chu, Electrochemical behavior Al_2O_3 /Al coated surgical AZ91 magnesium alloy in simulated body fluids, *J. Electrochem. Soc.* **155**, C178 (2008).
- [3] W. Zhang and J. R. Smith, Nonstoichiometric Interfaces and Al_2O_3 Adhesion with Al and Ag, *Phys. Rev. Lett.* **85**, 3225 (2000).
- [4] J. D. Baran, H. Grönbeck, and A. Hellman, Mechanism for Limiting Thickness of Thin Oxide Films on Aluminum, *Phys. Rev. Lett.* **112**, 146103 (2014).
- [5] N. P. de Leon, K. M. Itoh, D. Kim, K. K. Mehta, T. E. Northrup, H. Paik, B. S. Palmer, N. Samarth, S. Sangtawesin, and D. W. Steuerman, Materials challenges and opportunities for quantum computing hardware, *Science* **372**, eabb2823 (2021).
- [6] R. Winter, I. Krylov, C. Cytermann, K. Tang, J. Ahn, P. C. McIntyre, and M. Eizenberg, Fermi level pinning in metal/ Al_2O_3 /InGaAs gate stack after post metallization annealing, *J. Appl. Phys.* **118**, 055302 (2015).

- [7] S. Oh, K. Cicak, J. S. Kline, M. A. Sillanpää, K. D. Osborn, J. D. Whittaker, R. W. Simmonds, and D. P. Pappas, Elimination of two level fluctuators in superconducting quantum bits by an epitaxial tunnel barrier, *Phys. Rev. B* **74**, 100502 (2006).
- [8] L. Jiang, Z. Li, G. Fan, and D. Zhang, A flake powder metallurgy approach to Al₂O₃/Al biomimetic nanolaminated composites with enhanced ductility, *Scr. Mater.* **65**, 412 (2011).
- [9] N. Burgos, M. Paulis, M. Mirari Antxustegi, and M. Montes, Deep oxidation of VOC mixtures with platinum supported on Al₂O₃/Al monoliths, *Appl. Catal. B* **38**, 251 (2002).
- [10] A. V. Parmuzina and O. V. Kravchenko, Activation of aluminium metal to evolve hydrogen from water, *Int. J. Hydrogen Energy* **33**, 3073 (2008).
- [11] D.-G. Xie, Z.-J. Wang, J. Sun, J. Li, E. Ma, and Z.-W. Shan, In situ study of the initiation of hydrogen bubbles at the aluminium metal/oxide interface, *Nat. Mater.* **14**, 899 (2015).
- [12] S. N. Rashkeev, K. W. Sohlberg, S. Zhuo, and S. T. Pantelides, Hydrogen-induced initiation of corrosion in aluminum, *J. Phys. Chem. C* **111**, 7175 (2007).
- [13] Y. Liu, M. Alexander, E. Koroleva, P. Skeldon, G. E. Thompson, P. Bailey, T. C. Q. Noakes, K. Shimizu, and H. Habazaki, Detachment of alumina films from aluminium by 100 KeV H⁺ ions, *Surf. Interface Anal.* **33**, 318 (2002).
- [14] M. Li, D.-G. Xie, E. Ma, J. Li, X.-X. Zhang, and Z.-W. Shan, Effect of hydrogen on the integrity of aluminium-oxide interface at elevated temperatures, *Nat. Commun.* **8**, 14564 (2017).
- [15] D. R. Jennison, P. A. Schultz, and J. P. Sullivan, Evidence for interstitial hydrogen as the dominant electronic defect in nanometer alumina films, *Phys. Rev. B* **69**, 041405 (2004).
- [16] A. C. Kozen, M. A. Schroeder, K. D. Osborn, C. J. Lobb, and G. W. Rubloff, Examining the role of hydrogen in the electrical performance of in situ fabricated metal-insulator-metal trilayers using an atomic layer deposited Al₂O₃ dielectric, *Appl. Phys. Lett.* **102**, 173501 (2013).
- [17] J. C. Barbour, R. G. Copeland, R. G. Dunn, N. Missert, L. P. Montes, K.-A. Son, and J. P. Sullivan, The Electrical Properties of Native and Deposited Thin Aluminum Oxide Layers on Aluminum: Hydration Effects, No. SAND98-2534C (Sandia National Laboratories (SNL), Albuquerque, NM, 1998).
- [18] M. S. Khalil, M. J. A. Stoutimore, S. Gladchenko, A. M. Holder, C. B. Musgrave, A. C. Kozen, G. Rubloff, Y. Q. Liu, R. G. Gordon, J. H. Yum *et al.*, Evidence for hydrogen two-level systems in atomic layer deposition oxides, *Appl. Phys. Lett.* **103**, 162601 (2013).
- [19] A. M. Holder, K. D. Osborn, C. J. Lobb, and C. B. Musgrave, Bulk and Surface Tunneling Hydrogen Defects in Alumina, *Phys. Rev. Lett.* **111**, 065901 (2013).
- [20] L. Gordon, H. Abu-Farsakh, A. Janotti, and C. G. Van de Walle, Hydrogen bonds in Al₂O₃ as dissipative two-level systems in superconducting qubits, *Sci. Rep.* **4**, 1 (2014).
- [21] V. Somjit and B. Yildiz, Atomic and electronic structure of the Al₂O₃/Al interface during oxide propagation probed by ab initio grand canonical Monte Carlo, *ACS Appl. Mater. Interfaces* **14**, 42613 (2022).
- [22] See Supplemental Material at <http://link.aps.org/supplemental/10.1103/PhysRevMaterials.7.L072001> for additional details on simulation methodology, including interface model, DFT calculation parameters, calculation of defect formation energies and concentrations, and results from our Monte Carlo simulations.
- [23] J. Kang, J. Zhu, C. Curtis, D. Blake, G. Glatzmaier, Y.-H. Kim, and S.-H. Wei, Atomically Abrupt Liquid-Oxide Interface Stabilized by Self-Regulated Interfacial Defects: The Case of Al/Al₂O₃ Interfaces, *Phys. Rev. Lett.* **108**, 226105 (2012).
- [24] L. P. H. Jeurgens, W. G. Sloof, F. D. Tichelaar, and E. J. Mittemeijer, Structure and morphology of aluminium-oxide films formed by thermal oxidation of aluminium, *Thin Solid Films* **418**, 89 (2002).
- [25] D. L. Medlin, K. F. McCarty, R. Q. Hwang, S. E. Guthrie, and M. I. Baskes, Orientation relationships in heteroepitaxial aluminum films on sapphire, *Thin Solid Films* **299**, 110 (1997).
- [26] Z. Cheng, Y. R. Koh, H. Ahmad, R. Hu, J. Shi, M. E. Liao, Y. Wang, T. Bai, R. Li, E. Lee *et al.*, Thermal conductance across harmonic-matched epitaxial Al-sapphire heterointerfaces, *Commun. Phys.* **3**, 115 (2020).
- [27] G. Pilania, B. J. Thijsse, R. G. Hoagland, I. Lazić, S. M. Valone, and X.-Y. Liu, Revisiting the Al/Al₂O₃ interface: Coherent interfaces and misfit accommodation, *Sci. Rep.* **4**, 1 (2014).
- [28] D. Ma, Z. Lu, Y. Tang, T. Li, Z. Tang, and Z. Yang, Effect of lattice strain on the oxygen vacancy formation and hydrogen adsorption at CeO₂(111) surface, *Phys. Lett. A* **378**, 2570 (2014).
- [29] D. J. Siegel, L. G. Hector, and J. B. Adams, Adhesion, atomic structure, and bonding at the Al(111)/Al₂O₃(0001) interface: A first principles study, *Phys. Rev. B* **65**, 085415 (2002).
- [30] G. Kresse and J. Hafner, Ab initio molecular-dynamics simulation of the liquid-metal-amorphous-semiconductor transition in germanium, *Phys. Rev. B* **49**, 14251 (1994).
- [31] G. Kresse and J. Hafner, Ab initio molecular dynamics for liquid metals, *Phys. Rev. B* **47**, 558 (1993).
- [32] G. Kresse and J. Furthmüller, Efficiency of ab-initio total energy calculations for metals and semiconductors using a plane-wave basis set, *Comput. Mater. Sci.* **6**, 15 (1996).
- [33] G. Kresse and J. Furthmüller, Efficient iterative schemes for ab initio total-energy calculations using a plane-wave basis set, *Phys. Rev. B* **54**, 11169 (1996).
- [34] G. Kresse and D. Joubert, From ultrasoft pseudopotentials to the projector augmented-wave method, *Phys. Rev. B* **59**, 1758 (1999).
- [35] P. E. Blöchl, Projector augmented-wave method, *Phys. Rev. B* **50**, 17953 (1994).
- [36] J. P. Perdew, K. Burke, and M. Ernzerhof, Generalized Gradient Approximation Made Simple, *Phys. Rev. Lett.* **77**, 3865 (1996).
- [37] S. B. Zhang and J. E. Northrup, Chemical Potential Dependence of Defect Formation Energies in GaAs: Application to Ga Self-Diffusion, *Phys. Rev. Lett.* **67**, 2339 (1991).
- [38] C. G. Van de Walle, D. B. Laks, G. F. Neumark, and S. T. Pantelides, First-principles calculations of solubilities and doping limits: Li, Na, and N in ZnSe, *Phys. Rev. B* **47**, 9425 (1993).
- [39] H. Wipf, Solubility and diffusion of hydrogen in pure metals and alloys, *Phys. Scr.* **2001**, 43 (2001).
- [40] Y. Fukai, Metal-hydrogen system under extended *p*, *T* conditions, in *The Metal-Hydrogen System: Basic Bulk Properties*, edited by Y. Fukai (Springer, Berlin, 1993), Vol. 21, pp. 71–119.

- [41] H. Sugimoto and Y. Fukai, Solubility of hydrogen in metals under high hydrogen pressures: Thermodynamical calculations, *Acta Metall. Mater.* **40**, 2327 (1992).
- [42] C. Wolverton, V. Ozoliņš, and M. Asta, Hydrogen in aluminum: First-principles calculations of structure and thermodynamics, *Phys. Rev. B* **69**, 144109 (2004).
- [43] C. Freysoldt, B. Grabowski, T. Hickel, J. Neugebauer, G. Kresse, A. Janotti, and G. C. Van de Walle, First-principles calculations for point defects in solids, *Rev. Mod. Phys.* **86**, 253 (2014).
- [44] W. Tang, E. Sanville, and G. Henkelman, A grid-based Bader analysis algorithm without lattice bias, *J. Phys.: Condens. Matter* **21**, 084204 (2009).
- [45] E. Sanville, S. D. Kenny, R. Smith, and G. Henkelman, Improved grid-based algorithm for Bader charge allocation, *J. Comput. Chem.* **28**, 899 (2007).
- [46] S. Zhao, E. Kan, and Z. Li, Electride: From computational characterization to theoretical design, *WIREs Comput. Mol. Sci.* **6**, 430 (2016).
- [47] A. Janotti and C. G. Van de Walle, Hydrogen multicentre bonds, *Nat. Mater.* **6**, 44 (2007).
- [48] V. Somjit and B. Yildiz, Doping α -Al₂O₃ to reduce its hydrogen permeability: Thermodynamic assessment of hydrogen defects and solubility from first principles, *Acta Mater.* **169**, 172 (2019).
- [49] G. Zhang, Y. Lu, and X. Wang, Hydrogen interactions with intrinsic point defects in hydrogen permeation barrier of α -Al₂O₃: A first-principles study, *Phys. Chem. Chem. Phys.* **16**, 17523 (2014).
- [50] L. Ismer, M. S. Park, A. Janotti, and C. G. Van de Walle, Interactions between hydrogen impurities and vacancies in Mg and Al: A comparative analysis based on density functional theory, *Phys. Rev. B* **80**, 184110 (2009).
- [51] Y. F. Y. Fukai and N. Ō. N. Ōkuma, Evidence of copious vacancy formation in Ni and Pd under a high hydrogen pressure, *Jpn. J. Appl. Phys.* **32**, L1256 (1993).
- [52] Y. Fukai, M. Mizutani, S. Yokota, M. Kanazawa, Y. Miura, and T. Watanabe, Superabundant vacancy–hydrogen clusters in electrodeposited Ni and Cu, *J. Alloys Compd.* **356**, 270 (2003).
- [53] H. K. Birnbaum, C. Buckley, F. Zeides, E. Sirois, P. Rozenak, S. Spooner, and J. S. Lin, Hydrogen in aluminum, *J. Alloys Compd.* **253**, 260 (1997).
- [54] Y. Fukai, T. Haraguchi, E. Hayashi, Y. Ishii, Y. Kurokawa, and J. Yanagawa, Hydrogen-induced superabundant vacancies and diffusion enhancement in some FCC metals, *Defect Diffus. Forum* **194**, 1063 (2001).
- [55] R. Nazarov, T. Hickel, and J. Neugebauer, Ab initio study of H-vacancy interactions in fcc metals: Implications for the formation of superabundant vacancies, *Phys. Rev. B* **89**, 144108 (2014).
- [56] Y. Tateyama and T. Ohno, Stability and clusterization of hydrogen-vacancy complexes in α -Fe: An ab initio study, *Phys. Rev. B* **67**, 174105 (2003).
- [57] H. Saitoh, A. Machida, Y. Katayama, and K. Aoki, Formation and decomposition of AlH₃ in the aluminum-hydrogen system, *Appl. Phys. Lett.* **93**, 151918 (2008).
- [58] B. Baranowski and M. Tkacz, The equilibrium between solid aluminium hydride and gaseous hydrogen, *Z. Phys. Chem.* **135**, 27 (1983).
- [59] G. C. Sinke, L. C. Walker, F. L. Oetting, and D. R. Stull, Thermodynamic properties of aluminum hydride, *J. Chem. Phys.* **47**, 2759 (1967).
- [60] G. Lu and E. Kaxiras, Hydrogen Embrittlement of Aluminum: The Crucial Role of Vacancies, *Phys. Rev. Lett.* **94**, 155501 (2005).
- [61] C. G. Van de Walle and J. Neugebauer, First-principles calculations for defects and impurities: Applications to III-nitrides, *J. Appl. Phys.* **95**, 3851 (2004).
- [62] M. Youssef and B. Yildiz, Hydrogen defects in tetragonal ZrO₂ studied using density functional theory, *Phys. Chem. Chem. Phys.* **16**, 1354 (2014).
- [63] K. Carling, G. Wahnström, T. R. Mattsson, A. E. Mattsson, N. Sandberg, and G. Grimvall, Vacancies in Metals: From First-Principles Calculations to Experimental Data, *Phys. Rev. Lett.* **85**, 3862 (2000).
- [64] J. D. Fowler, D. Chandra, T. S. Elleman, A. W. Payne, and K. Verghese, Tritium diffusion in Al₂O₃ and BeO, *J. Am. Ceram. Soc.* **60**, 155 (1977).
- [65] M. Ichimura, Y. Sasajima, and M. Imabayashi, Grain boundary effect on diffusion of hydrogen in pure aluminum, *Mater. Trans. JIM* **32**, 1109 (1991).
- [66] J. Yamabe, S. Matsuoka, and Y. Murakami, Surface coating with a high resistance to hydrogen entry under high-pressure hydrogen-gas environment, *Int. J. Hydrogen Energy* **38**, 10141 (2013).
- [67] J. Towns, T. Cockerill, M. Dahan, I. Foster, K. Gaiher, A. Grimshaw, V. Hazlewood, S. Lathrop, D. Lifka, G. D. Peterson *et al.*, XSEDE: Accelerating scientific discovery, *Comput. Sci. Eng.* **16**, 62 (2014).
- [68] D. Stanzione, J. West, R. T. Evans, T. Minyard, O. Ghattas, and D. K. Panda, Frontera: The evolution of leadership computing at the national science foundation, in *Practice and Experience in Advanced Research Computing* (Association for Computing Machinery, New York, NY, 2020), pp. 106–111.